Available online at www.sciencedirect.com
SCIENCE DIRECT®
Journal of Electron Spectroscopy and Related Phenomena 141 (2004) 45–59
JOURNAL OF ELECTRON SPECTROSCOPY and Related Phenomena
www.elsevier.com/locate/elspec

Correction of non-linearity effects in detectors for electron spectroscopy

N. Mannella[a,b,*,1], S. Marchesini[b,2], A.W. Kay[a,b,3], A. Nambu[b,c], T. Gresch[b,d], S.-H. Yang[b,4], B.S. Mun[a,b,5], J.M. Bussat[e], A. Rosenhahn[b,6], C.S. Fadley[a,b]

[a] *Department of Physics, UC Davis, Davis, CA, USA*
[b] *Materials Sciences Division, LBNL, Berkeley, CA, USA*
[c] *Department Of Chemistry, University of Tokyo, Tokyo, Japan*
[d] *Institute of Physics, University of Zurich, Zurich, Switzerland*
[e] *Engineering Division, LBNL, Berkeley, CA, USA*

Received 8 October 2003; received in revised form 7 January 2004; accepted 7 March 2004
Available online 28 August 2004

Abstract

Using photoemission intensities and a detection system employed by many groups in the electron spectroscopy community as an example, we have quantitatively characterized and corrected detector non-linearity effects over the full dynamic range of the system. Non-linearity effects are found to be important whenever measuring relative peak intensities accurately is important, even in the low countrate regime. This includes, for example, performing quantitative analysis for surface contaminants or sample bulk stoichiometries, where the peak intensities involved can differ by one or two orders of magnitude, and thus could occupy a significant portion of the detector dynamic range. Two successful procedures for correcting non-linearity effects are presented. The first one yields directly the detector efficiency by measuring a flat-background reference intensity as a function of incident X-ray flux, while the second one determines the detector response from a least-squares analysis of broad-scan survey spectra at different incident X-ray fluxes. Although we have used one spectrometer and detection system as an example, these methodologies should be useful for many other cases.

Keywords: Photoemission spectra; Electron spectroscopy; Detectors; Non-linearity effects

1. Introduction

Electron detection systems are an integral part of any experimental setup for electron spectroscopy. Any deviation from an ideal linear response in which the true electron flux incident on the detector is not proportional to the response signal of the detector may cause undesirable effects in the recorded spectra. Seah et al. [1–3] have previously discussed methods for detecting non-linearity effects in photoelectron spectroscopy counting systems for spectra measured with laboratory X-ray sources. In this work, we develop methods for correcting for such non-linearities in a fully quantitative way.

Non-linearity is an ever-present concern in electron spectroscopy measurements. With laboratory X-ray excitation sources and solid samples, the differences between the highest and lowest photoelectron peak intensities can differ by as much as two orders of magnitude. Beyond this, for any electron spectrum, measurement of features in the higher-intensity low-energy secondary electron tail region of any spectrum can push many detection systems into non-linear behavior. For the particular case of synchrotron radiation ex-

* Corresponding author. Tel.: +(510) 495-2903; fax: +(510) 486-4299.
E-mail address: NMannella@lbl.gov (N. Mannella).
[1] Present address: Advanced Light Source, Lawrence Berkeley National Laboratory, MS7-100-1 Cyclotron Road, Berkeley, CA, USA
[2] Present address: LLNL, Livermore, CA, USA
[3] Present address: Intel Corporation, Portland, OR, USA
[4] Present address: IBM Almaden Research Laboratory, San Jose, CA, USA
[5] Present address: Advanced Light Source, LBNL, Berkeley, CA, USA
[6] Present address: Heidelberg University, Heidelberg, Germany

0368-2048/$ – see front matter © 2004 Elsevier B.V. All rights reserved.
doi:10.1016/j.elspec.2004.03.009

periments on solids, intensity levels can even more easily be found to exceed the linear response range of the detection systems. For example, several groups have observed non-linearity effects when using state-of-the-art photoelectron spectrometers such as for example the Gammadata/Scienta series of spectrometers [4–10]. In this situation, non-linearity effects are likely to be present when high-cross-section peaks are excited with bright sources (e.g. undulators), or even more so in resonant photoemission experiments during which photon energy is scanned [7]. For example, prior work on multi-atom resonant photoemission (MARPE) by several groups was strongly affected by non-linearity effects which produced irregularities in the size and shape of the measured resonances, with this effect arising through changes in the inelastic background underneath the peak whose intensity was being measured [4–10].

More generally, the possible occurrence of non-linearity effects should always be kept in mind whenever measuring relative intensities accurately is important, since it is not limited to resonance experiments. In fact, we have found for our example system that non-linearity effects are present even when the exciting energy is far away from any resonance and the countrates are relatively low, of the order of a few kHz. Examples of measurements significantly altered by non-linearity effects occurring at low countrates include quantitative analysis of complex oxides via core level intensities [11], relative intensities in angle-resolved valence spectra [12] and dichroism measurements on ferromagnetic systems [13].

In this paper, we explore in detail these non-linearity effects using photoemission intensities as an example, and focusing in particular on the response of the detector over the low countrate region. We demonstrate two quantitatively accurate correction procedures to correct for non-linearity effects. The first one directly yields the detector efficiency by measuring a flat-background reference intensity as a function of a linearly-varying incident X-ray flux, while the second determines the detector response from a least-squares analysis of broad-scan survey spectra, each of which spans a considerable fraction of the dynamic range, obtained at different incident X-ray fluxes. Although we have used one spectrometer system as an example (the Gammadata-Scienta SES200), the methodologies presented should be applicable to a broad array of situations.

2. Experimental

2.1. The detector system

We have performed our experiments using a Gammadata-Scienta SES200 spectrometer and detector system, as located on the advanced photoelectron spectrometer/diffractometer situated at the Berkeley Advanced Light Source [14,15]. The detection system used is that provided by the manufacturer as part of the standard equipment, and is schematically illustrated in Fig. 1. A microchannel plate multiplier (MCP) is followed by a phosphor screen at high voltage in ultra-high vacuum (UHV), so as to convert charge pulses into visible light pulses. A standard CCD camera [16], mounted outside the UHV chamber and focused on the phosphor screen through a glass viewport, is finally responsible for recording

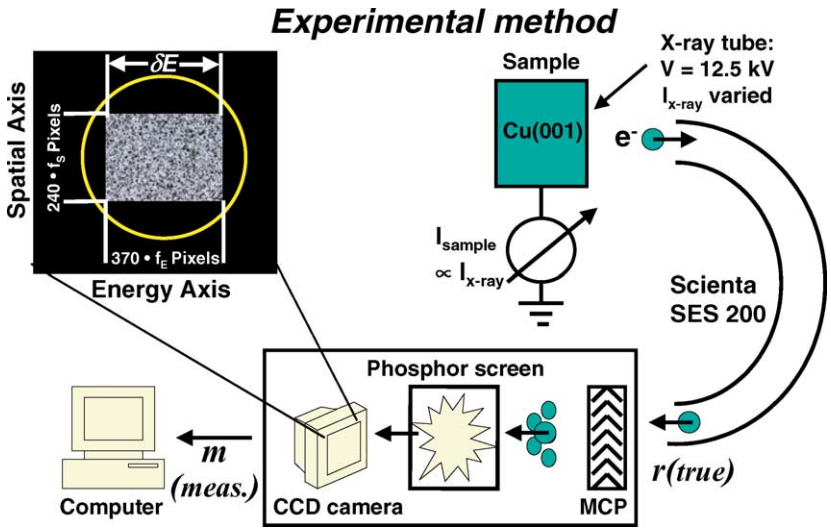

Fig. 1. Schematic illustration of the experimental geometry. The maximum active region of the detector (shown on the CCD camera monitor) includes 370 pixels along the energy axis and 240 pixels along the spatial axis, which is reduced to about 70,000 pixels via a rectangular window circumstribed by the circular microchannel plates and mating phosphor. Both the energy and spatial axis can be gated to include only a specific rectangular portion of the detector. The filling fractions f_E and f_S along the energy and spatial axis respectively can be set via software. Note that a linear variation in the X-ray emission current (at constant high voltage between filament and anode) results indeed in a linear increase in the flux of photons at the sample and thus of the electrons incident on the front of the MCP. In fact, the sample-to-ground current (in turn proportional to the photon flux at the sample), as measured with a picoammeter and recorded as a function of the X-ray emission current, has been found to track linearly with the emission current of the X-ray source at constant high voltage.

the light pulses on the phosphor and therefore performing the actual event detection. We have operated the detector primarily in the "*greyscale*" or "*analogue*" (GS) mode in which integrated CCD charge is used for counting, rather than in the "*black-and-white*" or "*digital mode*" (BW) in which individual pulses are counted. However, we also present some results based on the BW mode. In the GS mode, the readout involves a measurement of the collected charge in the pixel with an 8 bit analog to digital converter (ADC). For the GS mode, the equivalent of the BW mode discriminator is a digital mask that eliminates low-order ADC bits in an attempt to discard spurious noise counts. Further details have been reported elsewhere [4–6]. With any change in the discriminator levels or voltages across the MCP, the conditions under which the detector measures a count are altered and the response function will be modified. Unless otherwise explicitly specified, the detector has been intentionally used as delivered and installed by the manufacturer, leaving its settings at their recommended value at setup. However, in what follows, we will explore the influences of changing some of these settings on non-linearity.

This detector is intrinsically two-dimensional. The nature of the hemispherical energy analyzer to which the detector is attached results in one pixel axis of the camera representing the electron kinetic energy. The perpendicular axis, for our purposes, simply represents multiplexed detection at each energy. These axes will be referred to as the *energy* and *spatial* axis respectively (cf. Fig. 1). The camera views the 40 mm diameter circular phosphor screen, with the rectangle circumscribing this maximum active region of the detector including about 370 pixels along the energy axis (a number we will refer to as N_E) and 240 pixels along the spatial axis (a number we will refer to as N_S). Within a square circumscribing the circle, a maximum fraction, $\pi/4$, of the pixels within the square will actually include the phosphor screen image, leading to a maximum of approximately $370 \times 240 \times \pi/4 \approx 70{,}000$ pixels available for counting in two dimensions when the camera views the largest fully-filled rectangular image.

The detector operates in a mode for which both the energy and spatial axis can be gated to include only a specific rectangular portion of the detector in the final binned data: we will refer to the fractional coverage along the energy axis as f_E and that along the spatial axis as f_S. However, once these limits are selected, all counts for a given energy axis coordinate (i.e. a line of pixels along the spatial axis) are summed in hardware and only this binned sum is available for readout. This sum of spatial-axis pixels for a fixed energy pixel coordinate is referred to as a *detector channel*, whereas a pixel will refer to one pixel of the CCD camera.

In order to provide a detailed description of the detector response, the detected signal must first be processed from a typical distribution of total measured counts to a distribution of measured countrates *per pixel*. Once the detector signal has been acquired, the average countrate per pixel is computed as a function of the true countrate per pixel, revealing the response of the detector for the current detector settings (GS- or perhaps BW-mode, discriminator/mask setting, MCP and phosphor voltages).

The fact that the full camera image cannot be stored for analysis prevents the most accurate corrections of the effects to be considered here. That is, only in the limit of using a single pixel per detector channel can the actual per pixel countrate be obtained. However, we have dealt with this problem by gating the detector so as to have it count over only much smaller selected regions, as will be discussed further below.

The detector and analyzer can be run in two different modes, a *fixed* or *snapshot* mode as well as a *dithered* or *swept* mode. In the fixed mode, the analyzer settings determine the linear kinetic energy distribution over the energy axis of the detector and are held constant. For a given setting f_E, the detector will see a kinetic energy range of δE (cf. Fig. 1) that is a maximum of about 10% of the mean kinetic energy passed by the spectrometer. In this mode, the per-channel counts, which are actually sums of spatial pixel counts, are simply stored directly as read from the detector. By using only a narrow portion of the spatial axis over which the count-rate is nearly constant, the recorded counts may be trivially converted to a reliable per pixel countrate. For this particular case of data collected in the fixed mode, the correction from *per-channel* counts M to countrate per pixel m is given by

$$m = \frac{M}{\tau \times f_S \times N_S} \tag{1a}$$

where τ is the total dwell or counting time of the spectrum. Or, if we illuminate the detector with a uniform flux of electrons, then m can be obtained from the total countrate over all channels T via

$$m = \frac{T}{\tau \times f_E \times N_E \times f_S \times N_S} \tag{1b}$$

where τ is again the total dwell or counting time of the spectrum, $N_E = 370$ is the maximum number of active pixels along the energy-axis, f_E is the fraction of the detector that is filled along the energy axis, $N_S = 240$ is the maximum number of active pixels along the spatial axis, and f_S is the fraction of the detector that is filled along the spatial axis (cf. Fig. 1). Here, we have assumed that the filled portion of the spatial axis has essentially uniform countrate over the summed pixels. If this uniformity condition is not met, the efficiency may vary significantly across the spatial axis of the detector, and Eq. (1a) will give only some sort of average spanning a part of the dynamic range of the detector. The requirement of having uniform illumination over the active area of the detector can be experimentally achieved by using only a narrow portion of the detector along both the spatial and energy axis. The region of the detector over which counts are accumulated, indicated via the percentage of each of the two axis over which counting is permitted (f_E and f_S, along the energy and spatial axis, respectively), can be adjusted via software. A previous investigation provided evidence that there is no significant change

in the response function over any evenly illuminated surface of the detector, permitting us to much simplify the procedure for correcting spectra [4–6].

Normally, photoemission experiments are performed in a *dithered* or *swept* mode that involves sweeping the kinetic energy of the electrons accepted by the analyzer so that all energies in the final spectrum are accumulated in sequence by each channel in the detector. This is primarily done to allow parallel detection channels to be used while eliminating the channel-to-channel differences in the detector gain in the final spectra. For the dithered mode the correction from measured per-channel counts M to an average countrate per pixel m is given by an equation similar to Eq. (1a)

$$m = \frac{M}{\tau' \times f_S \times N_S} \tag{2}$$

where τ' is the total time that each pixel has spent in counting at each energy channel, as summed over the total number of sweeps [17].

2.2. Experimental methodology for detector characterization

In order to determine the response of the detector, one needs to determine the measured countrate as a function of the true countrate. To accomplish this in the most direct way, the true countrate, which is proportional to the number of electrons incident on the front face of the MCP, must be adjusted in a controlled manner while recording the measured countrate at the detector. Once the detector signal has been acquired, the average measured countrate per pixel is computed as a function of the true countrate per pixel, revealing the response of the detector for the used detector settings (GS or BW mode, discriminator/mask setting, MCP and phosphor voltages).

In this study, we have used electrons emitted during the photoemission process (photoelectrons) as a source of true countrates. Photoelectrons were provided by exciting with a standard laboratory X-ray source a Cu (1 1 0) single crystal in an "as-is" uncleaned condition, i.e. containing a stable amount of contamination in the UHV environment of the experiment. It is only important that the sample is in a stable condition during the duration of the measurements. We have in the present study used a standard X-ray tube (unmonochromatized dual-anode Al Kα/Mg Kα, Perkin–Elmer Model 04–548), which has a power supply permitting variable emission power which can be adjusted in 1 W steps at fixed high voltage.

We note that there is a fundamental question as to whether a linear variation in the X-ray emission current (at constant high voltage between filament and anode) results indeed in a linear increase in the flux of photons at the sample and thus of the electrons incident on the front of the MCP. We thus verified initially that the total electron current from the sample tracked linearly with the emission current of the X-ray source at constant high voltage. The sample-to-ground current (in turn proportional to the photon flux at the sample) was measured with a picoammeter and recorded as a function of the X-ray emission current, and thus also power since the voltage has been held constant (cf. Fig. 1). This relationship is found to be quite linear over the range of X-ray power used in this study (5–300 W), with all quadratic or higher-order terms contributing less than 5% of the linear component within this range, as already shown in a previous investigation [4]. Thus, using either the sample current or the X-ray power as a measure of the true countrate introduces negligible differences in the final response function analysis.

3. Results and discussion

3.1. The detection of non-linearity effects

Ideally, the behavior of the detector as a function of the true countrate should be completely linear. In this case, the detector response would be described as $m(r) = \varepsilon \times r$, where $m(r)$ and r denote the measured and the true countrate per pixel respectively, and ε is a counting efficiency factor. The constant ε would thus be equal to one in an ideal system, but it is for us only necessary to know it to within some constant factor. When the detector deviates from the ideal behavior, the detector response must be described by behavior, the detector response must be described by

$$m(r) = \varepsilon(r) \times r \tag{3}$$

where $\varepsilon(r)$ can be termed the *efficiency function* or *detector response function*, and it now depends on the true countrate, reflecting the deviation from ideal behavior. In order to correct measured countrates into true countrates it is necessary to determine the response function of the detector and invert Eq. (3). We note that since the signal is detected after being processed by the CCD camera, the values for the measured countrate (and, consequently, also for the true countrate) are not absolute, but are determined by the particular choice of the detector parameters (for example, discriminator threshold settings). Before discussing the procedures for the quantitative determination of this response function, we comment on a couple of straightforward ways to *detect* non-linearity effects by making use of survey spectra measured at different X-ray fluxes.

In Fig. 2(a) we show broad-range survey spectra collected in the dithered mode from a Cu (1 1 0) sample, as excited by Al Kα ($h\nu$ = 1486.6 eV) radiation. These spectra span countrates ranging from a few kHz to ≈ 12 MHz, corresponding to countrates per pixel in the range $m \approx 1$–240 Hz for the detector active area we have used. For our conditions of gating the active portion of the detector via f_S and f_E, the total number of active pixels is thus about 50,000, a number we will use in estimating total maximum uniform countrates later [18]. The same spectra are shown in Fig. 2(b) after they have been normalized with respect to the X-ray fluxes. If the detector

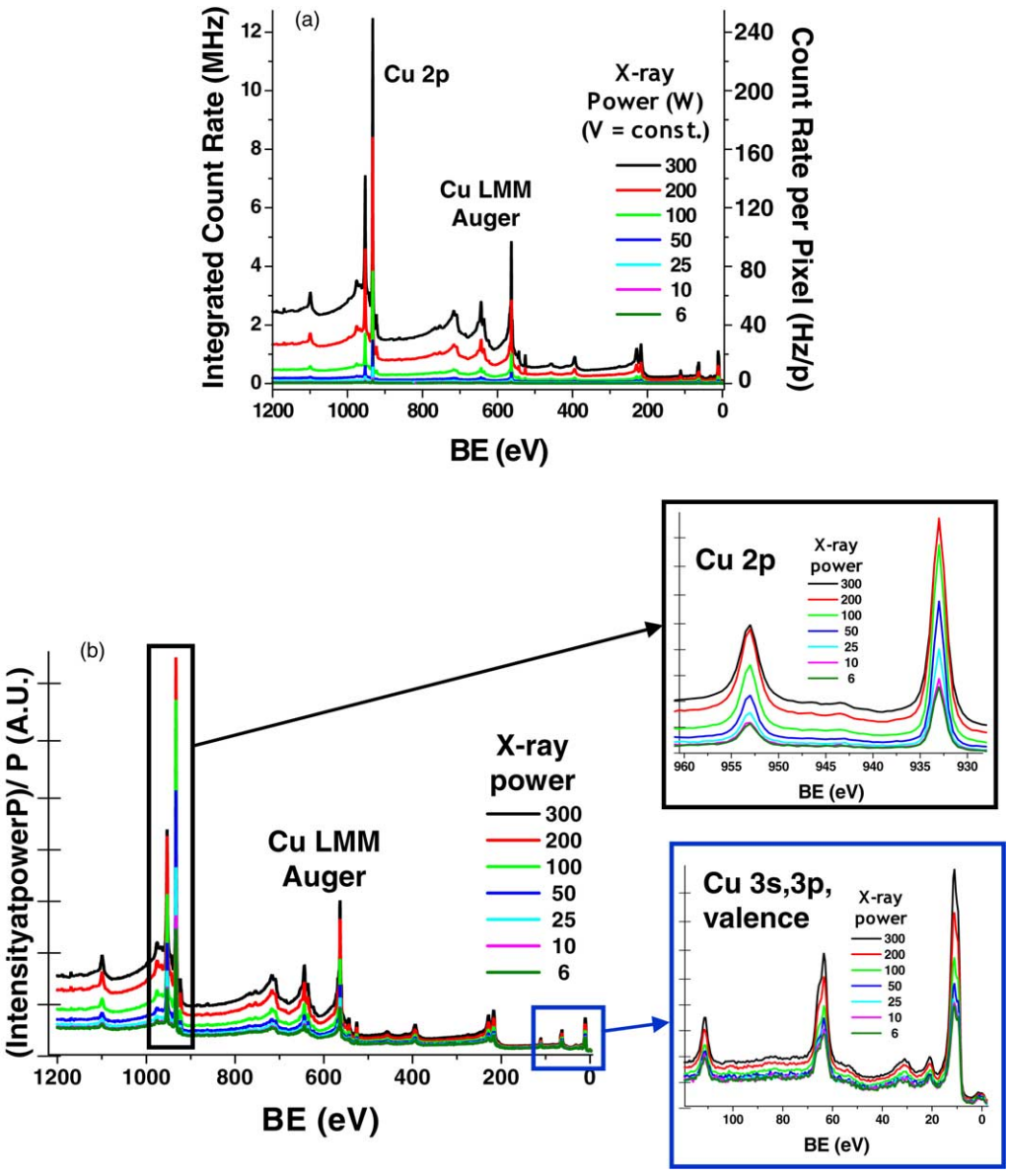

Fig. 2. (a) Broad-range survey spectra collected in the dithered (swept) mode from a Cu (1 1 0) sample, as excited by Al Kα ($h\nu$ = 1486.6 eV) radiation. Some more intense spectral features are labeled. Some weaker peaks result from a Ta clip at the edges of the Cu sample. The left ordinate here is an integrated rate assuming that 50,000 pixels count at the rate per pixel given on the right scale, and is this only appropriate to a situation of uniform illumination of the detector. (b) The same spectra as shown in (a) after they have been normalized with respect to X-ray flux. The fact that the spectra do not lie on top of one another provides unambiguous evidence for the presence of non-linearity effects.

were linear, all spectra in Fig. 2(b) should lie on top of one another, but it is evident that they are not, with factors of up to four separating them in the higher-intensity regions at higher binding energy (BE), as illustrated more quantitatively in the upper inset showing the Cu 2p spectral region. Even within the narrow binding energy range of 0–120 eV (lower inset), there can be differences of a factor of 2–3.

Another direct way to monitor non-linearity effects in electron detector systems makes use of "ratio plots", as introduced by Seah et al. [3], which consist of ratios of intensities in survey spectra measured at different X-ray fluxes. In Fig. 3, we plot the ratios of the uncorrected intensities of the individual spectral points collected at values of the X-ray power set to 300, 200, 100, 50 and 25 W and the intensity of the same spectral points in energy collected at 25 W. All intensities have been normalized by dividing by their respective X-ray emission currents, and the ratios are plotted versus the intensities of the relevant numerator spectrum. We note that the ratio plots are completely equivalent to plotting the ratios of the efficiencies curves as a function of the measured countrate. In fact, if two spectral points are recorded at two different emission currents related by a scaling factor n, from

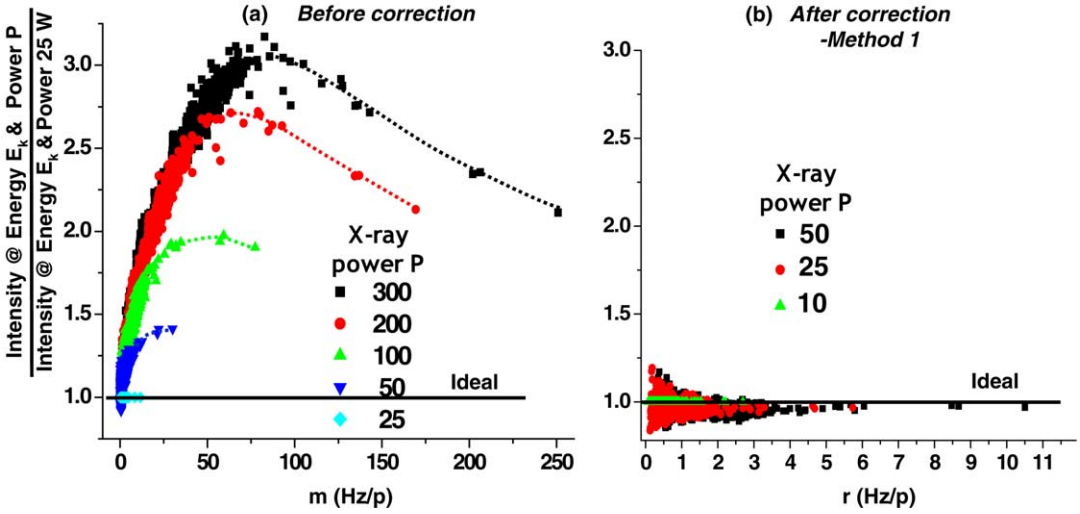

Fig. 3. Ratio plots (cf. [3]) of spectral intensities at a given kinetic energy and for different X-ray powers (equivalent to fluxes). The solid line indicates the behavior of an ideal linear detector with unit efficiency. (a) is before correction, and (b) after correction by Section 3.2. All points have been referred to the lowest power of 25 W (a) and 10 W (b). After correction, the ratio plots look like horizontal straight lines lying on top of one another, as expected in an ideal system. The deviation from a horizontal straight line shown for countrates approaching zero is simply due to the higher fractional statistical uncertainty that is typical of a Poisson distribution.

Eq. (3) we can write the ratio of the efficiencies as

$$\frac{\varepsilon(nr)}{\varepsilon(r)} = \frac{m(nr)}{n \times m(r)} = \left(\frac{m(nr)/nr}{m(r)/r}\right) \tag{4}$$

which shows that this ratio is equal to the ratio of the intensities of the two spectra normalized by the respective X-ray emission currents at which they have been collected. Ideally, the efficiency would have a constant value, so that the ratio in Eq. (4) should be constant. The main effect observed in Fig. 3 is that the ratios of the efficiency of the detector increase for measured countrates per pixel up to 60–70 Hz and decrease for countrates per pixel greater than 90 Hz, while in an ideal system one would expect these curves to be horizontal straight lines lying on top of one another, most simply of value unity, as shown in the figure.

We now consider two different methods for determining the response function of the detector and correcting nonlinearity effects. The first method directly yields the response function by measuring a flat-background reference intensity as a function of incident X-ray fluxes, while the second method determines the response function from what is effectively a least-squared-fit analysis of broad-scan survey spectra taken at different incident X-ray fluxes.

3.2. Correction method 1: measurement of flat-background reference intensity as a function of incident X-ray flux

The most obvious way to determine the response function of the detector is to record directly the measured countrate at the detector while adjusting the true countrate in a controlled manner. This is easily accomplished by measuring a flat-background region in a spectrum from a sample with a stable surface while varying the incident X-ray flux.

Although photoemission experiments are usually performed in a dithered mode, this mode was not used here because the inherent averaging over the detector would be detrimental to the analysis of the detector behavior. The analyzer and detector were on the contrary run in a fixed mode. Here we stress the importance of having uniform illumination over the active area of the detector in order not to have significant variations of the detector efficiency across the spatial axis of the detector. This requirement was experimentally achieved by setting via software the region of the detector over which counts were accumulated equal to 20 and 40% of the spatial and energy axis, respectively. The use of a featureless region of the spectrum (for example, for the Cu (1 1 0) sample shown in Fig. 2a, suitable regions would correspond to the binding energy ranges 134.6–164.6 and 850–900 eV) along with the use of a gated (40%) portion of the energy axis allows one to be able to measure several detector channels at the same time providing better statistics. The countrate per pixel can then be derived from Eq. (1a). For some of our measurements, a similar flat region in the spectrum from a $La_{0.7}Sr_{0.3}MnO_3$ sample was used in order to achieve higher intensities, as discussed in more detail below.

Once the detector signal has been acquired and converted to countrate per pixel, this method yields directly the response function of the detector as a function of the X-ray emission current or power, which is in turn proportional to the true countrate, as discussed before. By changing the operational mode of the analyzer (e.g. pass energy and slit size) of the analyzer, it was possible to derive the detector response in different regions of its dynamic range, thus permitting the measurement of various portions of the response function of the detector, particularly the one corresponding to less than 5 Hz per pixel. As previously shown [4–6], the only effect introduced by changing the settings of the analyzer is

simply a multiplication of the true countrate by a constant scaling factor. The nature of the scaling factor is immaterial to this discussion, but it must be compensated for in order to properly and self-consistently determine per pixel countrates.

Within each setting of the detector operational mode (e.g. GS or BW) and other detector and analyzer settings, the X-ray power was varied in the range 5–300 W (at fixed constant voltage $V = 12.5$ kV). We first combined several measurements of different portions of the response function corresponding to different operational mode settings into an overall measurement of the GS mode response function up to a measured rate of about 70 Hz per pixel (corresponding to a maximum total countrate over all energy channels of 3.5 MHz), as shown in Fig. 4. The data shown in Fig. 4 have been taken with a $La_{0.7}Sr_{0.3}MnO_3$ single crystal (containing a stable amount of contamination in the UHV environment of the experiment) and photoelectrons emitted from a featureless region with BE range 440–480 eV. This was done to obtain a measured rate of 70 Hz per pixel, e.g. higher than the 35–40 Hz per pixel which could be obtained from the Cu (1 1 0) sample, (cf. Fig. 2a).

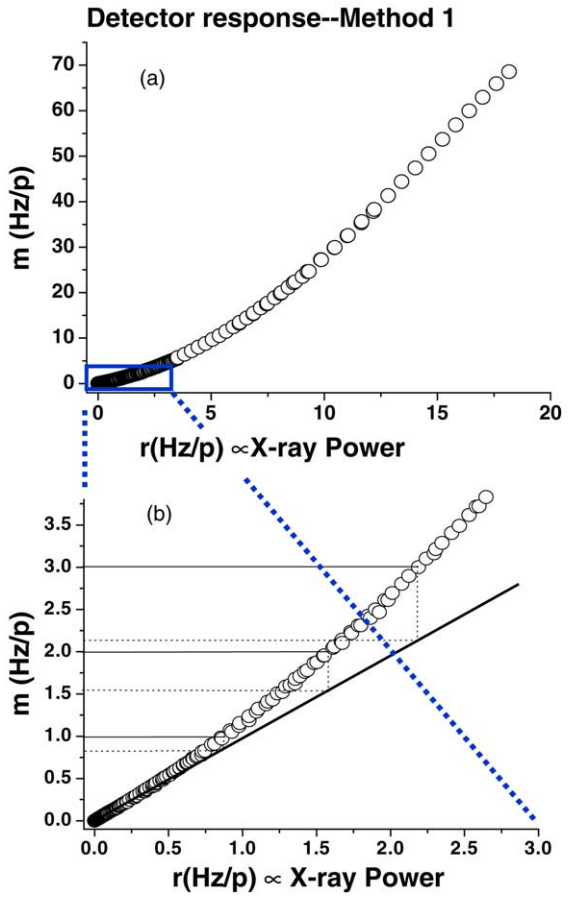

Fig. 4. (a) The detector response measured via the correction procedure of Section 3.2. Note the "quadratic" deviation from linearity at low countrates. (b) The detector response function for very low measured countrates (less than 3 Hz per pixel). Note that non-linearity effects are already present at measured countrates as low as 1 Hz per pixel.

Note that we generally do not know the point (if any) at which the measured and true countrates exactly coincide. In Fig. 4, we have arbitrarily set the true countrate scale so that the measured and true countrates are the same for count-rates approaching zero, with the asymptotic behavior of the measured detector response as the true countrate goes to zero being a straight line with slope equal to unity. This choice is of course equivalent to set the efficiency equal to unity at zero true countrate. It is important to realize that this choice is arbitrary, and that it does not affect the results of any correction we make.

Fig. 4 shows that the detector responds with significant deviations from the ideal linear behavior described by Eq. (3), *even at very low countrates*. This type of non-linearity for low countrates can approximately be described as a quadratic deviation from linearity, as previously observed for this particular detector in both GS and BW modes [4,6]. In particular, an inspection of Fig. 4(b) shows that the detector starts already to deviate from an ideal behavior at 0.5 Hz per pixel or a maximum countrate of 25 kHz. If we quantify the deviation from linearity as in $d = [m(r) - r]/r \times 100$, these data show that $d = 19$, 29 and 40% for measured countrates equal to 1–3 Hz per pixel, respectively.

Once the detector response function is determined, only a simple interpolation algorithm is needed to invert Eq. (3) so as to express the true countrates as a function of the measured countrates. It should also be noted that only after a spectrum has been corrected from measured to true countrate is a photon flux normalization appropriate.

Finally, we show in Fig. 5 the same spectral comparisons as in Fig. 2(b), but with and without the correction applied: it is clear that all normalized spectra for different fluxes coincide to a high accuracy (within 4.5% for all data points) after correction. Also, Fig. 3(b) makes the same point via the ratio plots. In fact, after correction, the ratio plots look like horizontal straight lines lying on top of one another, as expected in an ideal system. The deviation from a horizontal straight line shown for countrates approaching zero is simply due to the higher fractional statistical uncertainty that is typical of a Poisson distribution, which scales as the inverse of the square root of the counts. These results thus provide unambiguous evidence that the above-described procedure yields the correct determination of the response function and is effective in correcting non-linearity effects.

Nevertheless, an inspection of Figs. 3(b) and 5 reveals a minor inconvenience of this method. It has been possible to correct over the whole binding energy range only the spectra taken with X-ray powers of less than 50 W at most, corresponding to a maximum countrate of ≈70 Hz per pixel or ≈3.5 MHz maximum total countrate over all pixels. The cause for this limited range lies in the impossibility of finding a suitable featureless region in the spectra whose countrate is high enough to be able to drive the detector over a wider dynamic range [19]. Moreover, the necessity of adjusting in a controlled manner the incident

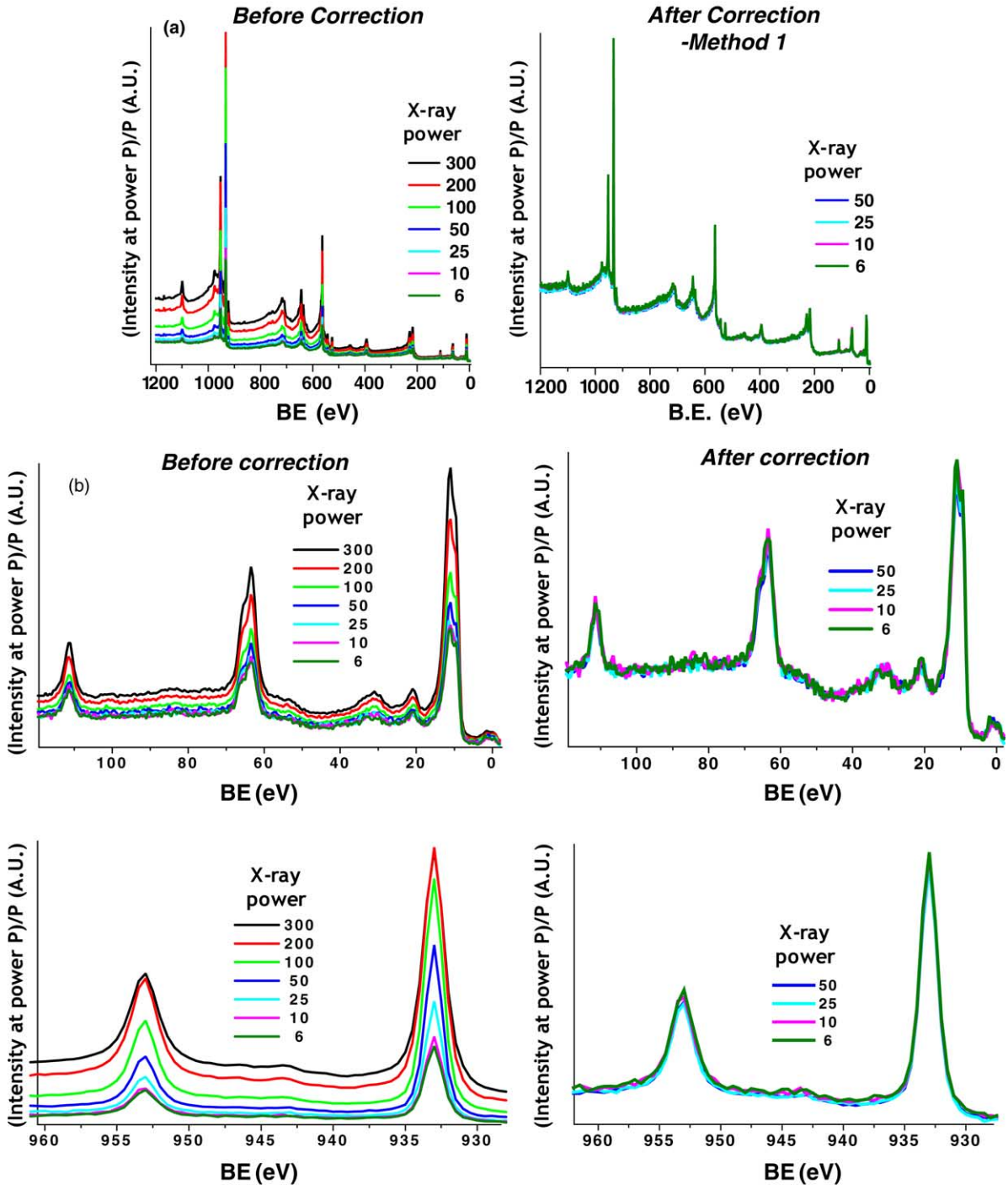

Fig. 5. The same spectra shown in Fig 2(b), but compared before and after detector non-linearity correction via Section 3.2. In (a), the full spectra are shown, and in (b) certain blowup regions. Note the limited power range possible with Section 3.2, going only up to about 70 Hz/pixel as measured.

X-ray flux can in principle impose stringent requirements on existing experimental setups. For example, standard X-ray tubes are not necessarily equipped with a power supply which allows quasi-continuous variation of the emission X-ray power (at constant voltage) with a stepsize as small as a few watts. Finally, combining several measurements of different portions of the response function of the detector by changing different operational mode settings into an overall measurement of the GS mode response function can be time-consuming. As an example, the collection of the several data sets combined in Fig. 4 took about 24 h. These considerations have motivated the development of an alternative procedure for correcting non-linearity effects that we now describe below.

3.3. Correction method 2: analysis of broad-scan survey spectra at different incident X-ray fluxes

The possibility to develop a new correction procedure was initially triggered by observing that a single broad-scan spectrum can provide in a single measurement a highly dense set of measured countrates. For example, Fig. 2(a) shows that the survey spectrum taken with the power set to 300 W yielded in a few minutes a distribution of measured countrate ranging from 0 to 240 Hz per pixel. The possibility of determining the detector response function from an analysis of survey spectra is thus appealing since it permits sampling a wide portion of the detector response in a relative short amount of time.

To make this idea more quantitative, consider a set of N survey spectra measured on the same sample, but with different incident fluxes $n = n_1, n_2, \ldots, n_N$, as shown in Fig. 2(a). For the case of data collected in the dithered mode, the one used to acquire the broad-scan survey spectra, the correction from per-channel count-rate M to count-rate per pixel m is given by Eq. (2). When expressed in countrate per pixel, the survey spectra provide a distribution of measured countrates $m = m(n_j, E_k)$ for a given X-ray flux n_j and kinetic energy E_K of the photoelectrons.

The true countrates per pixel $r(n_j, E_k)$ for a given X-ray flux and kinetic energy of the photoelectrons can now be expressed as a polynomial expansion of order P of the measured countrates per pixel $m(n_j, E_k)$ with real coefficients a_i

$$r(n_j, E_k) = \sum_{i=1}^{P} a_i \times m^i(n_j, E_k) \tag{5}$$

Here, we have set the coefficient a_0 (which represents the dark current background in the absence of any excitation) equal to zero, as this background is often negligible or can simply be measured and subtracted from all the measurements, but one can simply extend the summation to the 0th order term if necessary to include this. The determination of the response function and the correction of non-linearity effects are thus reduced to the computation of the unknown coefficients a_i's.

The *normalized* true countrates do not depend on the incident flux, such that we can write

$$\frac{r(n_1, E_k)}{n_1} = \frac{r(n_j, E_k)}{n_j} \tag{6}$$

From Eqs. (5) and (6), we can thus write out a system of $N - 1$ equations as

$$\frac{1}{n_1}\sum_{i=1}^{P} a_i \times m^i(n_1, E_k) = \frac{1}{n_j}\sum_{i=1}^{P} a_i \times m^i(n_j, E_k), \quad \begin{cases} \forall j = 2,3,\ldots, N \\ \forall k = 1, 2, \ldots, Q \end{cases} \tag{7}$$

where Q denotes the number of equally-spaced kinetic energy values used to collect the spectra.

As in our treatment of the first method, we have arbitrarily set the measured and true countrates to be the same at countrates approaching zero, which corresponds via this limit to setting the arbitrary value $a_1 = 1$. This still leads to a completely general result for the response function, since the true and measured counts can differ by an arbitrary factor. From Eq. (7) we then have with trivial rearrangement another system of equations

$$\underbrace{\frac{m(n_j, E_k)}{n_j} - \frac{m(n_1, E_k)}{n_1}}_{\boldsymbol{B}} = \underbrace{\sum_{i=2}^{P}\left[\frac{m^i(n_1, E_k)}{n_1} - \frac{m^i(n_j, E_k)}{n_j}\right]}_{\boldsymbol{C}} \times \underbrace{a_i}_{\boldsymbol{A}}, \quad \begin{cases} \forall j = 2, 3, \ldots, N \\ \forall k = 1, 2, \ldots, Q \end{cases} \tag{8}$$

In the matrix and vector notation introduced above, $\boldsymbol{A}$ is a $(P - 1)$ long column vector, $\boldsymbol{B}$ is a $Q \times (N - 1)$ long column vector, and $\boldsymbol{C}$ is a $Q \times (N - 1)$ by $(P - 1)$ matrix. Thus, in the ideal case for which there is no statistical error in the experimental data, $\boldsymbol{B} - \boldsymbol{CA} = 0$, and it would represent an over-determined set of equations for determining the coefficients a_i.

For the actual case with statistical variations in the data, Eq. (8) thus describe an over-determined system of $Q \times (N - 1)$ linear equations in the unknown $(P - 1)$ coefficients a_i's that can be solved for maximum likelihood by minimizing $|\boldsymbol{B} - \boldsymbol{CA}|^2$, i.e. solving the *normal equation* of the linear least-squares problem

$$\nabla_{\boldsymbol{A}}|\boldsymbol{B} - \boldsymbol{CA}|^2 = 2\boldsymbol{C}^T\boldsymbol{CA} - 2\boldsymbol{C}^T\boldsymbol{B} = 0 \tag{9}$$

where the superscript T denotes the transposition operation. The polynomial coefficients embedded in $\boldsymbol{A}$ can be obtained by standard methods such as the LU decomposition or simple matrix inversion [20] as

$$\boldsymbol{A} = (\boldsymbol{C}^T\boldsymbol{C})^{-1} \times \boldsymbol{C}^T\boldsymbol{B} \tag{10}$$

where $(\boldsymbol{C}^T\boldsymbol{C})$ is a small $(P - 1)$ by $(P - 1)$ matrix. For better numerical precision in the matrix inversion, we have rescaled the measured countrates per pixel m to vary from 0 to 1. Note that this overall approach is analogous to fitting the assumed polynomial form to the experimental data via a least-squares criterion. In practically implementing this scheme, we find that including powers up to $P \approx 12$ is necessary. The values of the other parameters for the results shown in this work are $N = 7$ and $Q = 2400$.

We have applied this fitting procedure to all the data points belonging to the survey spectra shown in Fig. 2(a). The detector response function has in this way been determined for measured countrates up to over 250 Hz per pixel (Fig. 6(a)),

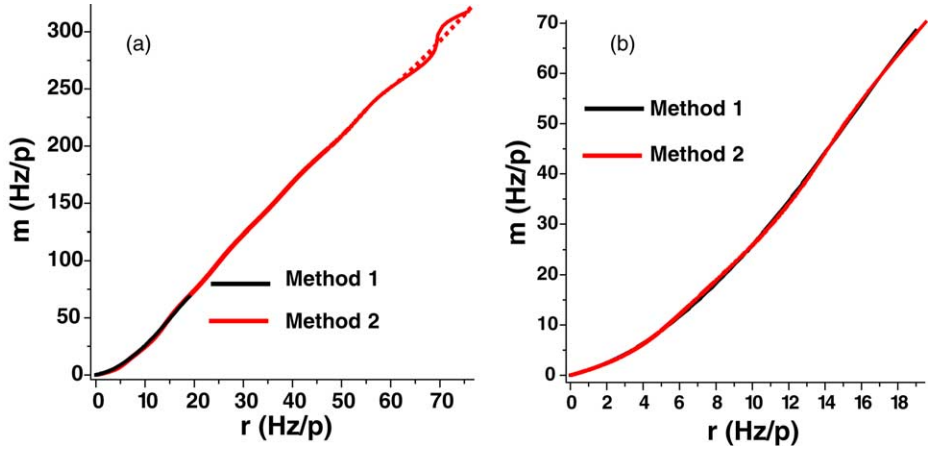

Fig. 6. Comparison of the detector response determined with correction methods 1 and 2. In (a), a broad range going up to above 300 Hz/pixel is shown, and in (b) only the more limited region in which the two methods overlap.

approximately a factor of 4 higher than the range accessed by the first method. Fig. 6(b) also shows that there is excellent agreement between methods 1 and 2 over the much narrower range covered by Section 3.2. We stress that in order to be able to invert Eq. (3), so as to determine the true counts r, the relationship m versus r must be a one-to-one mapping.

There is some deviation from a simple smooth curve in Fig. 6(a) above measured rates of approximately 260 Hz per pixel. This is simply due to the limited number of data points with countrate per pixel greater than the 250 accessible by our measurements. However, the smooth dashed curve in this region should permit correcting even up to about 325 Hz per pixel, corresponding to a total maximum countrate of 16.25 MHz.

We show in Fig. 7 the same spectra as in Fig. 2(b), but again comparing spectra with and without the correction procedure applied, this time via Section 3.3. All normalized spectra for different fluxes coincide to a high degree of accuracy (within at most 6% for all data points) over the entire range of the measured countrates accessed by the spectra shown in Fig. 2(a). This second correction procedure is thus very effective in correcting non-linearity effects and yields the correct determination of the response function for measured countrates extending to 250 Hz (or even 300 Hz) per pixel, approximately a factor of 4 higher than the range accessed by the first procedure.

Finally, we show in Fig. 8 the ratio plots shown in Fig. 3, but with the second correction procedure applied. After correction, the ratio plots look like one would expect in an ideal system, with the curves being horizontal straight lines lying on top of one another.

We suggest that this procedure will be particularly useful for existing experimental set-ups, such as those with standard X-ray tubes equipped with a power supply which can allow only a few X-ray emission current settings.

3.4. Further considerations

The correction procedures applied above clearly demonstrate successful and consistent methods for dealing with a non-ideal behavior in the response function of the detector. Maintaining a uniform illumination over the active portion of the detector screen is an essential condition for the effectiveness of both of the correction procedures described above. It should also be noted that there are alternate versions of the Gammadata/Scienta hardware that do allow full two-dimensional images to be retained in both energy and space and read out from the electronics interface. With these systems, it should be possible to apply the correction procedure developed here with even greater precision than that demonstrated here.

We have also successfully applied both correction procedures described above with variable photon flux provided by synchrotron radiation. In this particular situation, the variation in the photon flux at the sample can be monitored by recording the natural decay of the ring current (although this does not normally allow for more than a factor of 3 or so change in flux), or by changing the entrance (or exit) slits of the beamline while measuring either the photon flux along the beamline with a conventional "I_0" mesh or more directly the sample-to-ground total-electron-yield current. However, we point out that caution should be exercised to insure that changing the slits does not change the ratio between the beam spot size at the sample and the actual sample area seen by the spectrometer, otherwise a linear variation of the photon flux at the sample may not result in a linear increase of the number of electrons incident on the front of the MCP.

We stress that non-linearity effects should always be kept in mind for any case where measuring relative peak intensities accurately is important. As one illustration of this, we show in Fig. 9 the same spectra presented in Fig. 2(a) after the correction procedure has been applied. The overall countrate M and the countrate per pixel m now range from 0 to

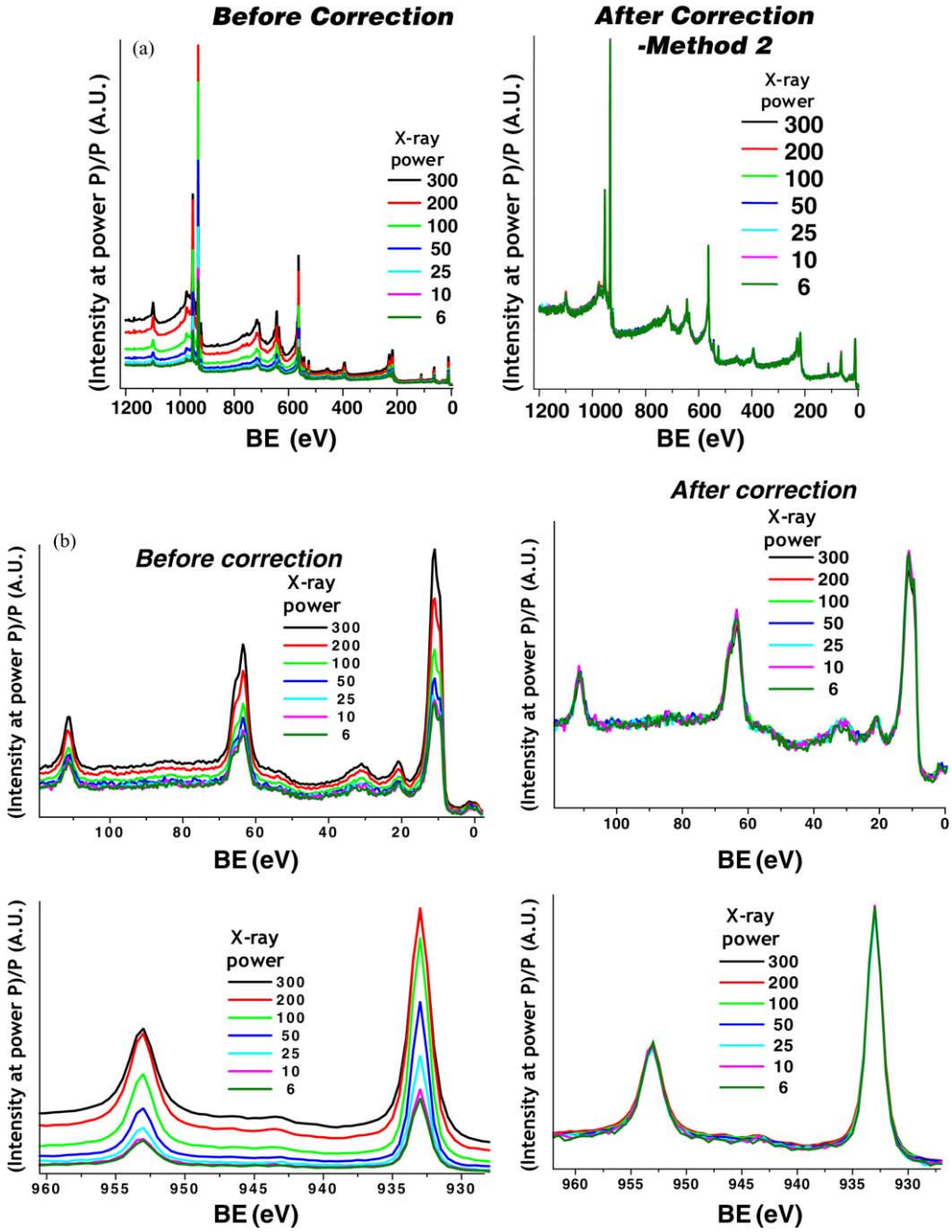

Fig. 7. As Fig. 5 but with correction via Section 3.3 – maximum likelihood fitting of a polynomial to broad-scan spectra via Eqs. 5–10. Note the similarity with Fig. 5 indicating that both correction procedures coincide and are effective in correcting for non-linearity effects. Note also the much broader power range for Section 3.3.

3 MHz and 60 Hz, respectively, that is, a factor of 4 less in range than before the correction has been applied. As a more concrete example of how quantitative analysis could be affected, Fig. 10 shows the ratio of the intensities of the Cu 2p and Cu 3s core level spectra, after taking into account differences in photoelectric cross section, electron attenuation lengths, and the transmission function of the analyzer, so as to effectively be taking a ratio of the Cu atomic density via two different spectra from the same atom. After the correction, as expected, this ratio is constant and equal to 1 within a full range of ±9%, while before the correction it shows a strong X-ray flux dependence and a value ranging from 1 to a little over 2.

As a final point, we note that all of the data reported to this point have been obtained with the detector intentionally used as delivered and installed by the manufacturer, leaving its settings at their recommended values at setup. We also note that several other groups appear to have encountered the same type of non-linearity with these standard settings [7–9]. According to the manufacturer's recommendations, a

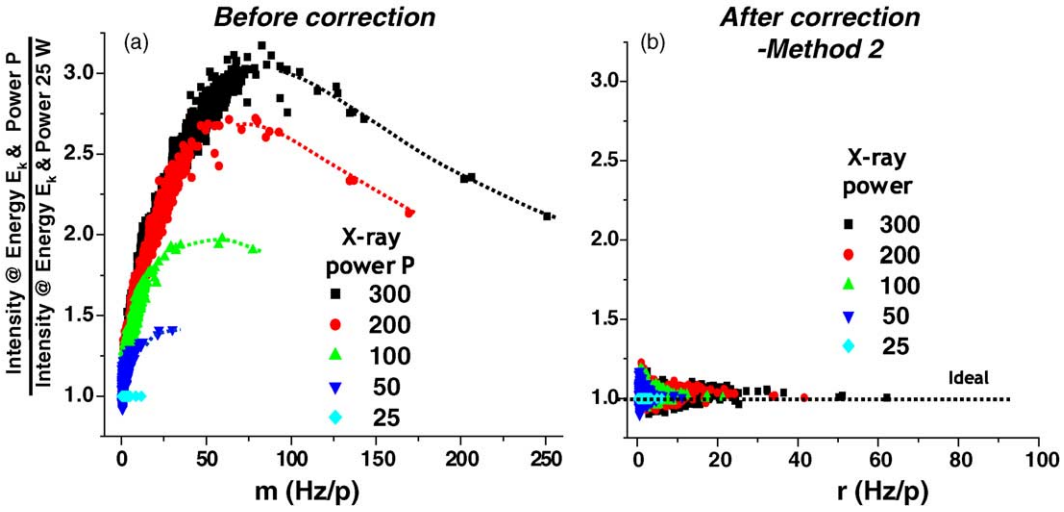

Fig. 8. As Fig 3, but with spectra compared (a) before and (b) after detector non-linearity correction via Section 3.3.

too-low discriminator level introduces noise, while a too-high discriminator level influences the detection efficiency of low intensity signals and therefore modifies the linearity of the intensity scale. The manufacturer recommends setting the discriminator by minimizing the dark counts; making sure that the dark counts are barely visible is thus thought to ensure that the discriminator is not set too high. As we discuss immediately below, we have in fact as part of this study varied both the discriminator setting and the phosphor and MCP high voltages, but the general type of non-linearity discussed here persists.

We thus now address the question of whether it is possible that the non-linearity effects so far observed are related to poor settings of the discriminator level. Seah et al. [1–3] have in fact pointed out that the discriminator setting in a detector very similar to ours can be used to improve linearity in certain countrate ranges, although this procedure is not expected to eliminate non–linearity effects over a broad countrate range, especially in GS operation due to the nature of this mode. In order to investigate whether an improper adjustment of the discriminator level on the detector could be held responsible for the non-linearity effects here reported, we thus studied the response function for various detector discriminator settings in both the GS and the BW modes. Making use of the first method described above, we determined the response functions corresponding to six different settings of the discriminator, with the results presented in Fig. 11. We deliberately used values for the discriminator setting (here reported as numbers in arbitrary units) lower and higher than that set by the manufacturer, which was equal to 314, so as to investigate what the effect of increasing or decreasing the threshold level

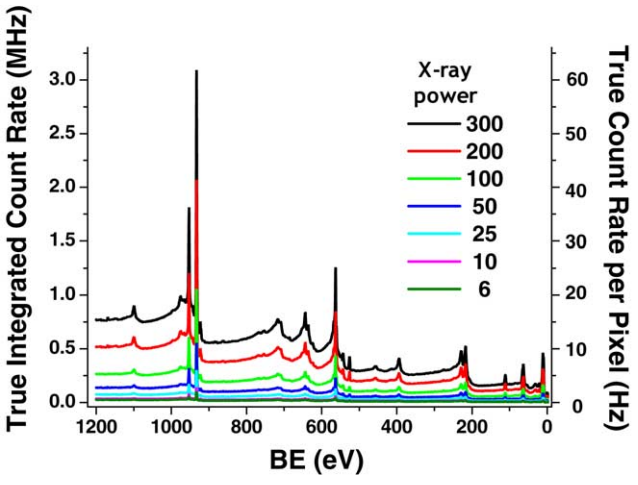

Fig. 9. The same spectra as in Fig. 2a after they have been corrected via Section 3.3. Note in particular that the maximum countrates per pixel or as integrated over all pixels after correction are a factor of 4 less than before the correction. The integrated total countrate assumes 50,000 active pixels uniformly illuminated, and may be optimistic in estimating maximum countrates achievable with this detector in the sense that spectra often have high countrate peaks well above background.

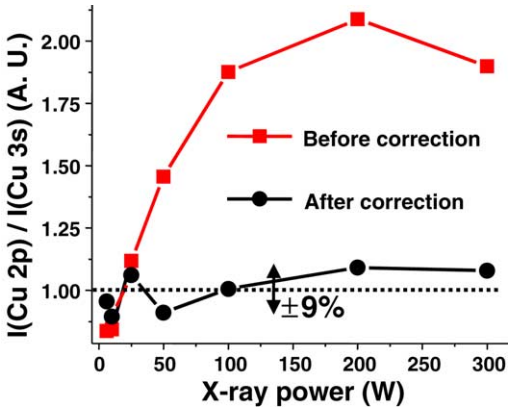

Fig. 10. The intensity ratio of the Cu 2p and Cu 3s core level spectra after allowing for the different photoelectric cross sections and electron inelastic attenuation lengths, as well as the transmission function of the analyzer, so as to yield a number that should in principle equal unity. Note the strong flux dependence of the ratio for the case of non-corrected spectra, a clear indication of the presence of non-linearity effects.

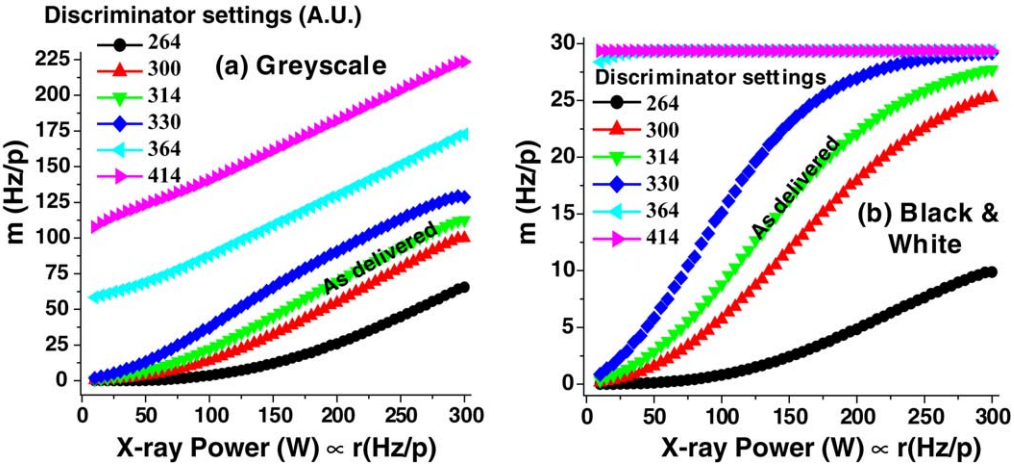

Fig. 11. The effects of changing the discriminator setting on the detector response function for the grey scale mode (a) and the black-and-white mode (b). All curves here show significant deviations from linearity.

would be. It is evident from an inspection of Fig. 11 that there is no value for the settings that we tried that yields the correct linear behavior over the entire countrate range accessed by our measurements. For the particular case of the GS mode, the discriminator settings which would allow one to measure spectra with quasi-linearity are those corresponding to the values 300, 314 and 330, centered on the manufacturer's recommended setting. Outside of this range, for the value equal to 264 we obtained a multi-valued response function, while for values equal to 364 and 414 the dark counts are so high that they would constitute an unacceptable noise level in the recorded spectra. For values equal to 300, 314 and 330, all three response functions show quadratic behavior at low countrates, as already pointed out before. In order to better quantify the deviation from an ideal linear behavior, we show in Fig. 12 (for the particular case of the GS mode) the detector responses corresponding to the discriminator values set to 300, 314 and 330 after they have been differentiated, i.e.

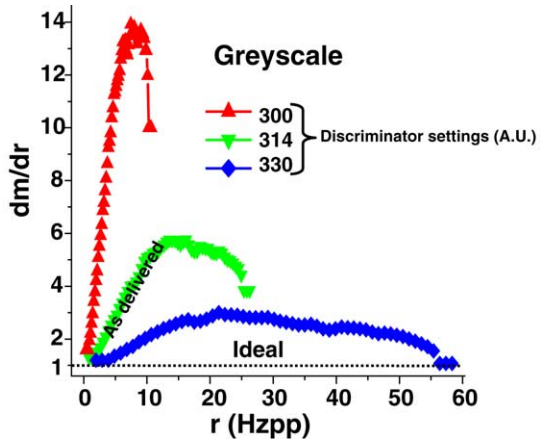

Fig. 12. The derivative of the detector response dm/dr obtained in the grey-scale mode (Fig. 11a) corresponding to the discriminator values of 300, 314 and 330. If the detector were linear, these should be horizontal lines.

d*m*/d*r*. Consistent with our prior analysis, we have arbitrarily set the true countrate scale so that the measured and true count-rates are the same for countrates approaching zero. The non-linearity affecting these response functions is evident: in an ideal case, these plots should be straight lines with zero slope. Therefore, these results indicate that it is generally unlikely that different discriminator settings would eliminate non–linearity effects for this particular detection system over a broad range of measured countrates normally accessed by typical photoemission measurements. Nonetheless, the setting of 330 in this figure is somewhat better than the 314 of the standard setup, even though it still shows a slope change of about a factor 3 over the range studied.

Beyond this, exploring optimum settings for detector high voltages, phosphor high voltages, and discriminators on our detection system is part of routine optimization of this detector, an operation performed approximately once a year on our system in collaboration with the manufacturer's engineers. We have recently verified that, just after re-optimizing (and in fact increasing) the MCP voltage, the detector still shows the same type of non-linearity, both qualitatively and quantitatively.

The detector response has also proven to be very stable over time. We obtained excellent reproducibility of the detector response (and hence correction procedure) even after 1 year, thus suggesting that the correction procedure does not have to be derived more often than once every six months or so, provided that the system is always operated at the same UHV conditions and the focus of the CCD camera is not changed.

Although a precise determination of the true source(s) of the non-linearity in this particular detector is beyond the scope of our paper, we briefly comment on the possible causes for the non-linearity effects we observe, first at high countrates and then at low countrates. Saturation of the detector at high countrates occurs most likely because of photon "pile-up" at the phosphor plate and/or saturation of the CCD camera

due to its maximum sampling rate. The photon "pile-up" at the phosphor occurs when the decay time of the phosphor is not sufficiently fast; for the phosphor used in our system the decay time is 10 μs, and thus we can estimate that pileup in a given pixel will begin to occur at about ten times the phosphor decay time or the equivalent rate of 10^4 Hz per pixel, a value which is much higher than any countrate measured in our work. The saturation of the CCD cameral is clearly shown in Fig. 11b for the spectra taken in black-and-white mode with the discriminator set to 364 and 414; in fact, for this particular model saturation occurs at 30 Hz per pixel (in black-and-white mode) since this is the CCD sampling rate.

It is not clear at the moment what the precise cause of the quadratic non-linearity at low countrate is, even though our investigation suggests that the most plausible source of these effects is the CCD camera. A too-low MCP high voltage would cause the gain to change sensitively as the flux change, giving rise to non-linearity effects. Nonetheless, we rule out a too-low MCP high voltage as a cause for the quadratic non-linearity, since after increasing the MCP the same non-linearity effects are found, as explained above.

It has been suggested that a change in the CCD camera might improve the behavior [21] of the detector, and this is a direction for future investigation. Plausible causes for the non-linear behavior at low countrates are CCD dark signal and CCD pattern noise. The first one is caused by some leakage currents which would produce charge in some of the pixels. It is expected that changing the discriminator values would suppress this source of noise, but our measurements (cf. Fig. 11) reveal that for different discriminator settings non-linearity effects are always present. CCD pattern noise refers to any pattern of counts (e.g. hot spots) which does not change significantly from frame to frame and, thus, even if not properly a random noise, can produce a dark signal-like background, however differing from random noise in that it would be dependent on the specific location of the CCD pixels used. As already noted above, we do not find any evidence on heterogeneity in the behavior of the pixels from one part of the detector to another, thus suggesting that CCD patttern noise cannot be held responsible for the non-linearity. From our investigation we conclude that most likely the cause of the non-linearity is the inherent use of a CCD camera, since such devices are well known to be non-linear devices [22], with the determination of the precise cause being object of future investigation.

More generally, this study constitutes a motivation for improving existing detectors and developing new detectors that overcome problems related to non-linearity effects over much larger countrate ranges.

4. Conclusions

We have developed two procedures for accurately correcting non-linearity effects in detectors for electron spectroscopy that should be applicable to a broad range of systems. The first one directly yields the detector efficiency by measuring a flat-background reference intensity as a function of incident X-ray flux, while the second one determines the detector response from a least-squares analysis of broad-scan survey spectra at different incident X-ray fluxes. To illustrate our correction procedures, we have characterized the detector response over a broad dynamic range of a state-of-the-art electron spectrometer system (Gammadata/Scienta SES200), using photoemission intensities as an example. Although we have studied only one spectrometer and detection system, our conclusions and general methods for determining and correcting for non-linearity are useful for many other cases. For the particular case studied here, our results demonstrate the occurrence of "quadratic" non-linearity effects which affect the detector response function at even very low countrates, far from saturation. Such non-linearity effects should thus always be kept in mind for any case where measuring relative peak intensities accurately is important, even at low countrates. Our results indicate that changing the discriminator settings does not eliminate these non-linearity effects, nor does adjusting the voltage across the multichannel plates. Finally, this study points out the importance of developing new detectors with a linear behavior over the entire countrate range accessed by typical experiments in electron spectroscopy.

Acknowledgement

This work was supported by the Director, Office of Science, Office of Basic Energy Sciences, Materials Science and Engineering Division, US Department of Energy under Contract No. DE-AC03-76SF00098.

References

[1] M.P. Seah, M. Tosa, Surf. Interface Anal. 18 (1992) 240.
[2] M.P. Seah, Surf. Interface Anal. 23 (1995) 729–732.
[3] M.P. Seah, I.S. Gilmore, S.J. Spencer, J. Electron Spectrosc. Relat. Phenom. 104 (1999) 73–89, The methods to check for linearity is described as ISO 212702003"Surface chemical analysis – X-ray photoelectron spectrometers and Auger electron spectrometers – linearity of intensity scale".
[4] A.W. Kay, Ph.D. dissertation, UC Davis, 2000.
[5] A.W. Kay, S.-H. Yang, E. Arenholz, B.S. Mun, N. Mannella, Z. Hussain, M.A. Van Hove, C.S. Fadley, J. Electron Spectrosc. Relat. Phenom. 114 (2001) 1179–1189.
[6] A.W. Kay, F.J.G. de Abajo, S.-H. Yang, E. Arenholz, B.S. Mun, N. Mannella, Z. Hussain, M.A. Van Hove, C.S. Fadley, Phys. Rev. B 63 (2001) 115119.
[7] M.G. Garnier, N. Witkowski, R. Denecke, D. Nordlund, A. Nilsson, M. Nagasono, N. Mårtensson, A. Föhlisch, Maxlab Annual Report for 1999. Lund, Sweden, and private communication.
[8] A. Nilsson, R. Denecke, et al., private communication.
[9] A. Kikas, E. Nommiste, R. Ruus, A. Saar, I. Martinson, Solid State Communications 115, (2000) 275, and A. Kikas, private communication.

[10] M. Finazzi, N. Brooke, private communication; G. Paolucci and K. Prince, private communication.
[11] N. Mannella, Ph.D. Dissertation, UC Davis, 2003.
[12] I.-D. Chang, D. Dessau, private communication.
[13] P. Wernet, N. Mannella, B. S. Mun, S.-H. Yang, C. S. Fadley, unpublished results.
[14] N. Mårtensson, P. Baltzer, P.A. Brühwiler, J.-O. Forsell, A. Nilsson, A. Stenborg, B. Wannberg, J. Electron Spectrosc. Relat. Phenom. 70 (1994) 117.
[15] C.S. Fadley, et al., J. Electron Spectrosc. Relat. Phenom. 75 (1995) 273.
[16] Manifactured by Sony, model XC-77 E72675, DC 10.5–15, vol. 2.2 W.
[17] The time τ' is a little more complicated to calculate, but if the active detector window in kinetic energy is δE (cf. Fig. 1), then the smallest reasonable step in kinetic energy (or equivalently energy channel width) will be $dE = \delta E/(f_E N_E)$. If the spectral region to be scanned is ΔE in width, (where ΔE is usually $\geq \delta E$), then, in order to have each detector pixel contribute equally to each energy channel, the detector has to be scanned over a range of $\Delta E + \delta E$, involving a maximum no. of energy steps $S = (\Delta E + \delta E)/dE = (\Delta E + \delta E) f_E N_E/\delta E$. If the actual accumulation time at each energy step is $\delta\tau$, not including any time necessary for the saving of data and settling in of the power supplies, and the spectrum is swept F times, then the total time τ' to accumulate a swept-mode spectrum will be $\tau' = FS\delta\tau$. If, as is often the case, a certain number of detector energy channels α is binned together to make a final spectral energy channel of width αdE, where $\alpha > 1$ and need not be an integer, then the number of energy steps is reduced to $S' = S/\alpha$ and the total time becomes $\tau' = FS\delta\tau/\alpha$.
[18] The filling fractions f_E and f_S along the energy and spatial axis have been set to 0.8 and 0.7, respectively. Consequently, one has $0.8 \cdot 370 \cdot 0.7 \cdot 240 \approx 50000$ as a conversion factor between countrate per pixel and overall maximum total countrate (T/τ), provided the detector sees a uniform illumination (see Eq. (1b)).
[19] Changing the sample could help in some cases, even though it is unlikely to find a featureless region which can provide countrates as high as 240 Hz per pixel.
[20] W.H. Press, S.A. Teukolsky, W.T. Vetterling, B.P. Flannery, Numerical Recipies in C: the art of scientific computing, second ed., Cambridge University Press, 1992.
[21] P.D. Johnson, private communication.
[22] Y. Reibel, M. Jung, M. Bouhifd, B. Cunin, C. Draman, Eur. Phys. J. AP 21 (2003).